THE ASTROPHYSICAL JOURNAL, 171:213–231, 1972 January 15

PHOTOIONIZATION AND THE EMISSION-LINE SPECTRA OF QUASI-STELLAR OBJECTS*

KRIS DAVIDSON
Princeton University Observatory, Princeton, New Jersey
Received 1971 July 12; revised 1971 August 23

ABSTRACT

Detailed photoionization calculations are used to examine the information conveyed by relative emission-line intensities in QSO spectra. It is found that the elemental abundances cannot be estimated with any assurance; but if "conventional" values are assumed, then certain restrictions may be placed on the ionizing spectra and gas densities. In particular, the ratio between radiation density and gas density is determined. Narrow filaments or sheets of ionized gas seem to be indicated; these may be compressed regions behind shock fronts.

I. INTRODUCTION

This paper is an account of some calculations made in an effort to partially interpret the emission-line spectra of quasi-stellar objects (QSOs). The line-emitting gas is assumed to be photoionized by continuum radiation, which must be produced by some unspecified mechanism somewhere in the QSO. The calculated models illustrate possible elemental abundances, ionizing spectra, and gas densities which together can reproduce a "typical" QSO spectrum.

Since the early discussion by Greenstein and Schmidt (1964), various authors have considered the ionized gas associated with QSOs. Osterbrock and Parker (1966) and Mathez (1969) attempted to derive temperatures and densities in line-emitting regions directly from the observed line intensities, using assumed values for the abundances of the various ion species. Shklovskii (1965) suggested that a stratified model might be appropriate, and Burbidge *et al.* (1966) proposed a fairly detailed qualitative scheme in which progressive absorption of ionizing photons in successive frequency ranges may produce distinct zones containing ions at different stages of ionization.

Bahcall and Kozlovsky (1969*a*, *b*) have calculated the stratified ionization equilibria in regions with assumed uniform temperatures which are illuminated by central photon sources with power-law spectra. Since the electron temperature at each point is assumed rather than calculated from local heating and cooling rates, the line intensities and especially the effects of collisional ionization are not fully consistent in these models. Tarter, Tucker, and Salpeter (1969) and Tarter and Salpeter (1969) have described calculations which include thermal balance, and in which some attempt has been made to allow for the behavior of secondary ionizing photons. These models do not simulate a QSO spectrum in detail, but they are very useful as general guides to the arrangement of highly ionized regions, and are closely related to the models described in this paper. Other calculations, not directly related to QSO spectra but qualitatively relevant, have been made by Williams (1967).

In the models discussed below, an attempt is made to reproduce the emission-line intensities appropriate to a composite "typical" or "average" (and therefore somewhat hypothetical) QSO, presumed to be at a cosmological distance. The assumed configuration of the gas is spherically symmetric, with a central source of ionizing photons. If the gaseous shell is geometrically thin, it may approximate a system of filaments or thin sheets—provided that some allowance is made for the escape of ionizing photons between

* Much of this work was done as part of a Ph.D. thesis at Cornell University.

filaments or sheets. (Such details of geometry do not greatly affect the results of the present discussion.) At each point in the gas, the ionization-and-temperature equilibrium is found from the local radiation-density spectrum. The transfer of ionizing radiation is treated by an iterative procedure. Some of the physical parameters (e.g., photoionization cross-sections and dielectronic recombination coefficients) are probably improved over those used by Tarter *et al.* (1969) and Bahcall and Kozlovsky (1969*a*, *b*). The calculative procedure is described in § II below.

Section III describes the observed and adopted emission-line intensities, while § IV lists a few implications which are evident without extensive calculation. The computed models are described in §§ V and VI; in § V, the elemental abundances are "conventional" (i.e., resembling normal galactic values), while § VI considers the possible reduction of helium or heavier-element abundances. Finally, § VII discusses the physical situation of the gas as indicated by the various models.

II. METHOD

Calculations were made with a computer program, previously mentioned by Davidson and Tucker (1970), which is a descendant of that developed by Tarter (1967) but with improved physical processes and a different treatment of radiative transfer.

Given the gas density, abundances, photoionization cross-sections, and recombination and cooling coefficients, the equilibrium ionization and temperature at a point may be calculated from the local radiation-density spectrum, as described, for example, by Williams (1967). Certain processes such as recombination may produce secondary ionizing radiation, whose distribution must depend upon the state of the gas. In order to find distributions of radiation, ionization, and temperature which are mutually consistent, an iterative approach is employed rather in the manner of Williams. The assumed central source produces a continuous radiation spectrum above $\nu = 1$ Ryd.[1] This flux is incident upon the spherical inner boundary of the gas; and as a first guess, radiation is traced outward through the configuration by calculating the state of the gas, absorption, and reemission at each point while pretending that all secondary and scattered radiation moves outward. Thus is obtained a preliminary estimate for the state of the gas, from which a resulting secondary radiation distribution may be computed, properly including inward-moving photons (see Appendix). Then a second iteration is possible, tracing the primary photon flux outward again but now using the previously estimated distribution for the secondary and scattered photons. This yields an improved estimate of the state of the gas, and the next iteration follows similarly. In favorable cases this procedure eventually converges toward self-consistency. Only two or three iterations were used in each model described below, because the secondary radiation is in each case less important than the relatively straightforward primary flux.

The elements H, He, C, N, O, and Ne were included, and in some cases Mg II–IV were considered in a simplified fashion. For hydrogenic and helium-like ions, photoionization cross-sections were calculated from the Stobbe formulae (Bearden 1966)—except for He I, for which values given by Bell and Kingston (1967) were used. For heavy ions, contributions for removal of inner-shell electrons were included by using Stobbe formulae for each shell at high frequencies; while near thresholds for ions with $2p$ electrons, the adopted cross-sections approximated those listed by Henry and Williams (1968), Hidalgo (1968), and Seaton (1958). Typical accuracies may be of the order of 20 percent. For Mg II, Biermann and Lübeck (1949) have described the rather small cross-section

[1] Although the word "frequency" is used for convenience, in this paper the symbol ν actually denotes photon energy, so that Planck's constant may be omitted from the formulae and a flux spectrum F_ν has the convenient dimensions (energy/energy-area-time), while the parameter U_1 defined in § IV has velocity-like dimensions. As a unit of energy, 1 Rydberg = 13.6 eV = 2.18×10^{-11} ergs, corresponding to a frequency of 3.29×10^{15} Hz.

for removal of the $3s$ electron; and just beyond the $2p$ threshold at $\nu = 5$ Ryd, the cross-section probably rises to perhaps 5×10^{-18} cm^2 by analogy with neon.

Adopted radiative and dielectronic recombination coefficients were approximately equal to those used by Cox and Tucker (1969) and Tucker (1969). In certain models discussed below, dielectronic recombination involving carbon and oxygen ions is significant. Therefore, an important consideration is the possible reduction of dielectronic recombination rates at high electron densities (Dupree 1968). From the work of Allen and Dupree (1969) and Burgess and Summers (1969), it seems possible that C IV $\rightarrow$ C III dielectronic recombination is suppressed for $n_e \gtrsim 10^7$ cm^{-3}. Unfortunately, this is quite uncertain without detailed calculations.

Parameters for free-electron cooling by collisional excitation of ions were adapted from various sources, discussed by Bely and Van Regemorter (1970). (It is worth noting that the collision strength for excitation of the C III] λ1909 line, according to Osterbrock (1970), is several times larger than that used in previous discussions of QSO spectra.) Since high densities, temperatures, and photon fluxes were present in each model, fine-structure cooling was neglected (see Bahcall and Wolf 1968). Free-free cooling and thermal collisional ionization were included; coefficients for the latter have been listed by Cox and Tucker (1969).

Secondary ionizing radiation with a continuous spectrum may be produced by electron-ion recombination or by free-free emission. In addition, some ions can produce ionizing emission lines. All of these contributions were included in the radiative transfer, although only the hydrogen and helium recombination emission is really important. Rather than attempt to allow for resonance scattering, the resonance-line photons were simply added to the appropriate continuum-frequency intervals. In the case of the He II Lα line ($\nu = 3$ Ryd), this may cause some error in the distribution of temperature in He II and He III zones.

Finally, hydrogen-oxygen charge transfer was assumed to correlate the first-stage ionization of hydrogen and oxygen so that n(O II)/n(O I) $\equiv 8n$(H II)/$9n$(H I) (see Field and Steigman 1971). This relation was used to find the O II/O I ratio, rather than using the O I photoionization and recombination rates.

III. OBSERVED LINE INTENSITIES

Table 1 is a list of relative intensities of the brighter emission lines in eleven QSO spectra, adapted from estimates by several observers. Pairs of forbidden lines involving the same terms have been combined, e.g., [O III] $\lambda\lambda$5007 + 4959 together are denoted λ5007; this convention will be followed throughout the discussion. Possible absorption features will be neglected.

Far-ultraviolet lines are observable only when redshifted into the visual range, i.e., in the spectra of the more distant objects; but in such cases the longer-wavelength lines have not been measured. Relative intensities of ultraviolet and visual lines for different objects must therefore be compared by some indirect procedure. In Table 1, this is done by normalizing the small-redshift spectra so that $I(\mathrm{H}\beta) = 1$, and large-redshift spectra so that $I(\mathrm{L}\alpha) = 40$. These values should be consistent if the hydrogen lines are caused by recombination, plus a relatively small collisionally excited contribution to Lα—as in most of the models to be described. However, one must remember that the proportion of Lα which is collisionally excited is not known observationally. The absolute Lα luminosities of objects included in Table 1 probably range between 3×10^{44} and 3×10^{45} ergs s^{-1}, while the visual-continuum luminosities are several times larger.

If all of the major emission lines between 1000 and 7000 Å are to be considered in a model, it is necessary to adopt a composite "typical" spectrum such as that listed in Table 2. This set of relative intensities is intended to represent a crude average or sum-

TABLE 1

A. Relative Emission-Line Intensities in QSO Spectra*

Spectral Line	3C 273 (z=0.158)	3C 321.1 (z=0.264)	3C 249.1 (z=0.311)	PKS 2251+11 (z=0.322)	3C 48 (z=0.367)	3C 286 (z=0.848)	CTA 102 (z=1.037)
C III] λ1909	..	..	...	..		0.6	2†
Mg II λ2798	0.25	1.7†	2.5	0.9	0.3	0.45	2†
[Ne V] λ3426	.	0.5†	0.5:	.	0.2	..	. .
[O II] λ3727	.	.	<0.3	.	0.3	..	.
[Ne III] λ3868	. .	.	.	.	0.2:	..	.
[O III] λ4363	..	.	0.1:	..	..	. .	.
He II λ4686	<0.03	..	0.3	<0.1	<0.1	.	.
H I λ4861	1.0	1†	1 0	1.0	1.0	1.0	1†
[O III] λ5007	0.35	1†	2.0	0.7	2.0	2.8	1†
H I λ6563	2.6	7†	6.7	5.8	..	. .	.
References.	*abcg*	*e*	*de*	*de*	*aeg*	*e*	*e*

Note.—A blank space does not necessarily imply the absence of a line. Also, certain related lines have been combined, e.g., [O III] λ5007 + λ4959.

* Smaller redshifts, normalized to Hβ = 1.

† Indicates I(λ5007) = I(λ4861) by assumption, where only the total is known.

B. Observed Ultraviolet Lines, Normalized to Lα = 40

Spectral Line	PHL 938 (z=1.930)	3C9 (z=2.012)	PKS 0237−23 (z=2.202)	4C05.34 (z=2.877)
H I λ1215	40	40	40	40
C IV λ1549	10	8	7.6	11
He II λ1640	< 4	4	6	4
C III] λ1909	2.2	.	.	...
References	*deg*	*eg*	*eg*	*f*

References. *a* = Greenstein and Schmidt 1964; *b* = Oke 1965; *c* = Wampler and Oke 1967; *d* = Wampler 1968; *e* = Oke *et al.* 1970; *f* = Oke 1970; *g* = Bahcall and Oke 1971.

TABLE 2

A Composite QSO Line Spectrum*

Line	Relative Intensity	Line	Relative Intensity
H I λ1215	40.0	[O II] λ3727	0.2:
C IV λ1549	9	[Ne III] λ3868	0.4:
He II λ1640	≤ 3	[O III] λ4363	≤0.2
C III] λ1909	2	He II λ4686	≤0.3
Mg II λ2798	1.5	H I λ4861	1.0
[Ne V] λ3426	0.4:	[O III] λ5007	2

* Adapted from Table 1 above, and Table 3 4 of Burbidge and Burbidge (1967).

mary of the data in Table 1. Such an averaging procedure is obviously perilous, since there may be distinct classes of QSO spectra and since certain sets of lines may be negatively correlated. Indeed, the He II recombination lines may indicate a systematic difficulty: theoretically $I(\lambda 1640)/I(\lambda 4686) \sim 8$, and so in Table 1 these lines seem to be more prominent in the more distant QSOs than in those with smaller redshifts. An additional problem is possible reddening by dust, which may be indicated by the observed Balmer-line ratios; however, the ultraviolet-visual normalization may have partly compensated for such reddening.

These difficulties having been noted, the following discussion will be an attempt to reproduce Table 2 through calculated models.

IV. SOME PRELIMINARY CONSIDERATIONS

The continuous spectrum of a typical QSO, extrapolated to ionizing frequencies, is sufficient to show that photoionization must be an important heating mechanism in the associated line-emitting gas. Some additional excitation may be due to fast particles (see Bergeron and Souffrin 1971); but to avoid extreme complication, the following discussion will suppose that the only energy input to the gas is a continuous spectrum of ionizing photons—this is not implausible, since Table 2 is at least qualitatively similar to the spectrum of a photoionized region. For purposes of discussion the elemental abundances are first *assumed* to be similar to ordinary galactic values; likely modifications will be mentioned parenthetically or will become evident in §§ V and VI. Under these conditions the emission lines provide some immediate information.

Some of the forbidden lines are weaker (relative to Hβ) than in more familiar galactic nebulae. At a conventional temperature below 20,000° K, and at low densities with conventional abundances, the collision strengths are such that the [O III] λ5007 line should be more intense than C IV λ1549 (which originates in the same ionization zone as λ5007); but this is not the case in Table 2. Several explanations are possible:

1. Carbon may be considerably more abundant than oxygen—in which case the C IV λ1549 line might become the most effective cooling mechanism. However, in this paper as in most previous discussions, drastic variations of *relative* C, N, O, and Ne abundances will not be considered, for the additional parameters would make the problem too indeterminate for convenient discussion.

2. The temperature of the gas might be high—above 25,000° K—favoring the higher-excitation lines, C IV λ1549 in particular. But for almost any reasonably smooth ionizing spectrum, the assumed abundances provide sufficient cooling to preclude such high temperatures in the O III, C IV zone. To obtain high temperatures it is necessary to reduce the cooling efficiency by reducing heavy-element abundances—probably by factors of the order of 10 or more.

3. The electron density may be high enough to reduce forbidden-line intensities by collisional de-excitation. With conventional abundances and a temperature near 15,000° K, $n_e \sim 3 \times 10^6$ cm^{-3} would explain the low $I([\text{O III}]\ \lambda 5007)/I(\text{C IV}\ \lambda 1549)$ ratio in Table 2. However, [O III] λ4363 is not suppressed at this density and would have the maximum intensity allowed by Table 2; and for certain objects (such as 3C 249.1—see Table 1) this value is too large. The forbidden [Ne III] line might also be uncomfortably intense. Thus, in order to adjust several lines simultaneously, it is appropriate to consider a slightly more complicated model in which the density is nonuniform. The simplest such model involves two components. In the denser component ($n_e > 3 \times 10^6$ cm^{-3}), [O III] λ5007 is severely reduced by collisional de-excitation while λ4363 may be somewhat reduced, depending upon the density; this gas is favorable for the production of C IV λ1549. The low-density component is invoked to produce the desired [O III] λ5007 intensity with only slight additional contributions to λλ1549 and 4363. Support for such a two-component model may perhaps be found in at least one QSO spectrum

where the [O III] λλ5007 and 4363 lines have different widths (Burbidge and Burbidge 1967). In any case, a two-component model is the simplest representation of nonuniformities that are likely to occur. It is true that a single-component model with $n_e \sim 10^6$ cm^{-3} is possible if the oxygen/carbon and neon/carbon abundance ratios are reduced below "normal" values; but in such a model the temperature and the parameter U_1 would not be very much different from the dense models in § V below, so this might be regarded as a special case in which the components merge.

Other line ratios provide hints about radiation densities. Suppose that an ionization-limited H II layer is formed on the edge of a cloud of gas by an incident radiation flux spectrum F_ν. If F_1 denotes F_ν at $\nu = 1$ Ryd, then, for a given spectrum shape, a very useful parameter is $U_1 = F_1/n_e$. This quantity determines various characteristics of the ionized region: the optical thickness, the degree of ionization $[n(H^+)/n(H^0)$ at any point], and the sharpness of stratification into zones containing different stages of ionization. However, the *relative* sizes of the different ionization zones depend only upon the shape of the ionizing spectrum and are nearly independent of U_1, at least in cases where the stratification is reasonably distinct. If F_ν extends to high frequencies, the zones occur as follows (Burbidge *et al.* 1966; Tarter and Salpeter 1969): (1) Directly exposed to the radiation is a zone where H II, He III, O IV, O V, O VI, and other multiply ionized species predominate. (2) In the next zone, where there are only a few photons beyond $\nu = 4$ Ryd, the principal ions are H II, He II, C IV, N III, O III, Ne III, and Mg III. (This will be the most important zone in the following discussion.) (3) The gas beyond the ionization front, having few photons above $\nu = 1$ Ryd, may consist of H I, He I, C II, N I, O I, Ne I, and Mg II. However, a few penetrating X-ray photons may partly ionize the heavy elements.

The above scheme is valid unless the helium abundance is either quite large (Davidson and Tucker 1970) or very small (Bahcall and Kozlovsky 1969*a*); the latter possibility will be discussed later below. The immediate points of interest in the stratification scheme are that C III is nowhere a major constituent, and that Mg II occurs only in the H I region where line excitation is difficult. Thus, in order to explain the C III] λ1909 and Mg II λ2798 lines, it is apparently necessary to choose a value of U_1 which is sufficiently small for some C III and Mg II to coexist with C IV and Mg III in zone 2. In a two-component model, such a low value of U_1 is most easily assigned to the denser gas.

The relative intensities of C IV λ1549 and Lα provide an independent estimate of U_1. Consider a region where U_1 and n_e are large. Since the forbidden lines are collisionally suppressed, the C IV line accounts for much of the free-electron cooling and so represents a crude measure of the absorbed energy flux; while Lα is due to recombination and so measures the absorbed photon flux. Hence the ratio $I(\lambda 1549)/I(\mathrm{L}\alpha)$ is determined chiefly by the slope of the ionizing spectrum (or the average ionizing photon energy). But if U_1 is decreased, the concentration of neutral hydrogen within the H II region increases until, for some value of U_1, collisionally excited Lα becomes appreciable. This increases the total Lα intensity; furthermore, it decreases the intensity of C IV λ1549, since the collisionally excited Lα now accounts for some of the cooling of the free electrons. Therefore, $I(\lambda 1549)/I(\mathrm{L}\alpha)$ is found to decrease for sufficiently small values of U_1. Since this line ratio is in fact surprisingly small in Table 2, it is natural to suspect that U_1 can be estimated by this method.

Finally, the He II λλ1640 and 4686 lines may give information about the shape of the ionizing spectrum, as noted by Williams (1971). The intensities of these recombination lines are proportional to the extent of the He III zone and therefore to the flux of incident photons above $\nu = 4$ Ryd. The number of absorbed photons above $\nu = 1$ Ryd is similarly represented by the Hβ line (whose collisionally excited portion is probably negligible, unlike Lα). The ratio $I(\mathrm{He\ II}\ \lambda 4686)/I(\mathrm{H}\beta)$, for a complete, ionization-limited H II region, is thus found to depend upon the slope of the ionizing spectrum but not upon the helium abundance. This statement becomes invalid for a very low helium

abundance—less than perhaps 0.01 relative to hydrogen, depending upon the ionizing spectrum. In such a case, He III extends throughout the ionized region and most of the photons beyond $\nu = 4$ Ryd are absorbed near the ionization front by hydrogen rather than helium; then $I(\lambda 4686)/I(H\beta)$ becomes small and proportional to the helium abundance. The models by Bahcall and Kozlovsky (1969*a*, *b*) are of this type.

The considerations outlined above are important and useful in selecting parameters for QSO models. Quantitative details will be illustrated in the following two sections.

V. MODELS WITH CONVENTIONAL ABUNDANCES

The term "conventional abundances" here implies a similarity to the Population I or Disk Population II abundances which have been assumed in most previous discussions of QSO spectra. The models described in this section all assume the following values, relative to hydrogen, by number: He = 0.07; (C, N, O, Ne, Mg) = (1.2, 0.6, 2.5, 0.6, 0.1) $\times 10^{-4}$. These are rather low by Population I standards; but according to calculations not described here, larger values tend to be less satisfactory for simultaneously explaining Lα, C IV λ1549, and C III] λ1909 intensities.

The gas is assumed to have two density components. Models 1 and 2 are plane-parallel calculations representing the denser component, which presumably takes the form of a thin shell, or more likely, a collection of clouds, filaments, or sheets of gas, each optically thick in the Lyman continuum. This component may intercept perhaps 10–50 percent of the ionizing radiation produced in the QSO (see Oke, Neugebauer, and Becklin 1970). The lower-density component, illustrated by Model 3, is used primarily to account for [O III] λ5007. This component may be uniform or nonuniform, and may be optically thin except in the helium Lyman continuum just above $\nu = 4$ Ryd.

The input parameters for Models 1 and 2 differ only in the adopted ionizing spectra. Constant gas pressure is assumed in each case, with rather high electron densities of the order of 10^8 cm^{-3}; so all of the major forbidden lines are severely affected by collisional de-excitation. Also because of the high densities, dielectronic recombination has been neglected, as mentioned in § II above. (The one important effect of this rather uncertain detail is to decrease the C III/C IV ratio by a factor of 2 or 3 in both models; in fact, this is found to make agreement with Table 2 easier to obtain.)

The ionizing spectra for Models 1 and 2 are shown in Figure 1. Here F_ν represents the energy-flux spectrum of a beam of photons normally incident upon a sharp boundary of the plane-parallel configuration. Model 1 uses a power-law spectrum, $F_\nu \sim \nu^{-1.4}$, with

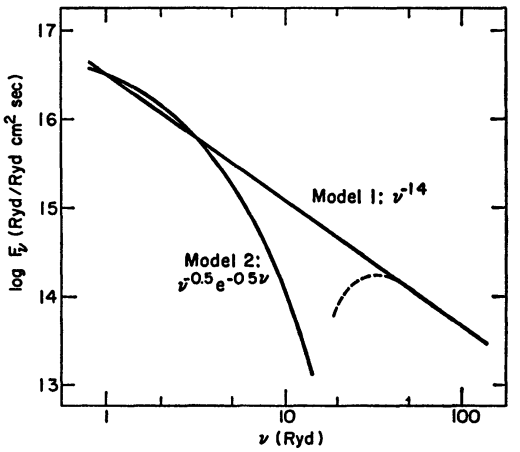

FIG. 1.—Ionizing spectra incident upon Models 1 and 2 (see § V). *Dashed line*, X-ray flux which penetrates beyond $z = 1.4 \times 10^{13}$ cm in Model 1.

$F_1 = 3.3 \times 10^{16}$ Ryd Ryd^{-1} cm^{-2} s^{-1}. The total energy flux above $\nu = 1$ Ryd is 1.8×10^6 ergs cm^{-2} s^{-1}—this might represent, for example, a source whose ionizing luminosity is 10^{45} ergs s^{-1}, as seen from a distance of 2.2 pc. In Model 2, the spectrum steepens at high frequencies, $F_\nu \sim \nu^{-0.5} e^{-0.5\nu}$, and is equal to the other spectrum at $\nu = 1$ Ryd. The total ionizing flux in Model 2 is 9.5×10^5 ergs cm^{-2} s^{-1}. The ultraviolet slopes of both spectra are fairly consistent with observed near-ultraviolet spectra of various QSOs (Oke *et al.* 1970).

Figures 2–6 show characteristics of the ionized gas in Models 1 and 2, as functions of distance z from the illuminated boundary. The hydrogen densities and electron temperatures are shown in Figure 2, while Figure 3 shows the ionization of hydrogen and helium. In each case, the thickness of the ionized region is of the order of 10^{13} cm—a remarkably small dimension, which will be discussed in § VII below. The He III zone is fairly extensive, and the He III–He II boundary is ill defined in Model 1, which has a relatively large flux of high-frequency photons. Penetrating X-ray photons cause significant ionization of helium and heavier elements in the H I zone of this model. Figure 4 shows carbon ionization; by design, the C III/C IV ratios are roughly similar in the two models. Oxygen and neon ionization in Model 2 are shown in Figure 5. In Model 1 (not shown), neon remains ionized beyond the H II–H I boundary but oxygen becomes mostly neutral because of charge exchange with hydrogen. Finally, the approximate amount of Mg II in each model is shown in Figure 6. Since the photoionization cross-section of Mg II is assumed to be relatively large beyond 5 Ryd (the $2p$-shell threshold), Mg II is much less abundant in Model 1 than in Model 2.

In Table 3 are listed the relative intensities of the major emission lines produced by Models 1 and 2 (except for a few hydrogen and helium recombination lines). As an

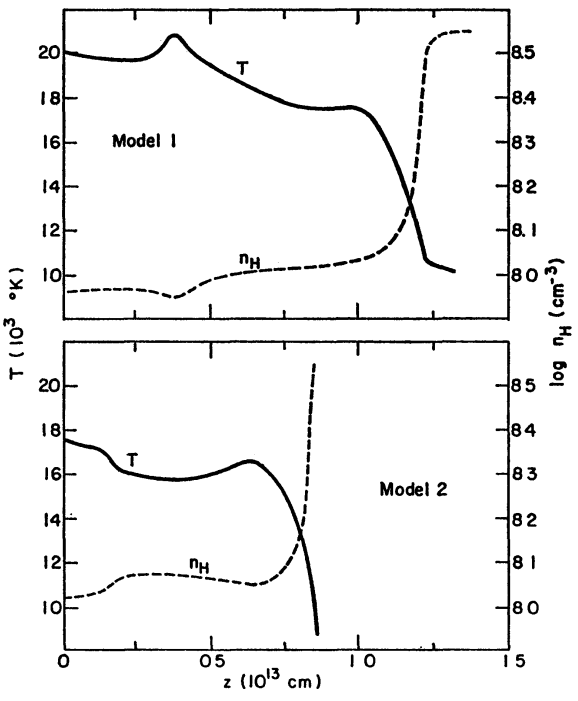

FIG 2

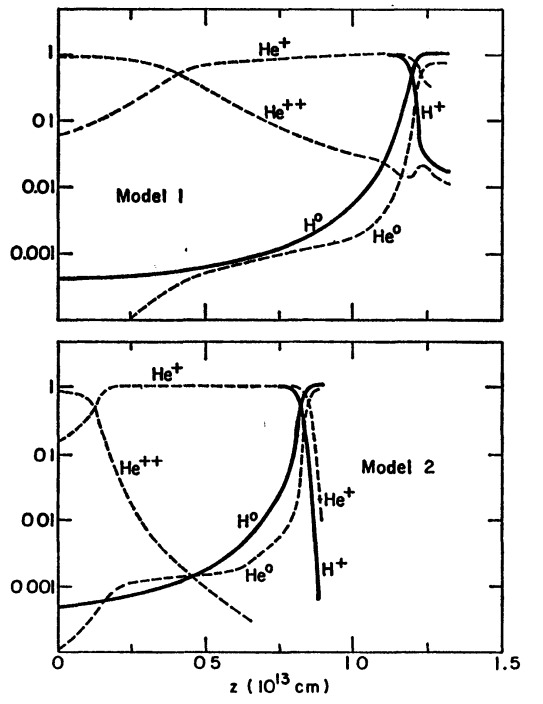

FIG 3

FIG. 2.—Temperatures and hydrogen densities as functions of position z in Models 1 and 2. These are plane-parallel, constant-pressure models.

FIG. 3.—Ionization of hydrogen and helium in Models 1 and 2. Ordinate represents the fraction of each element which occurs at a given ionization stage at each point.

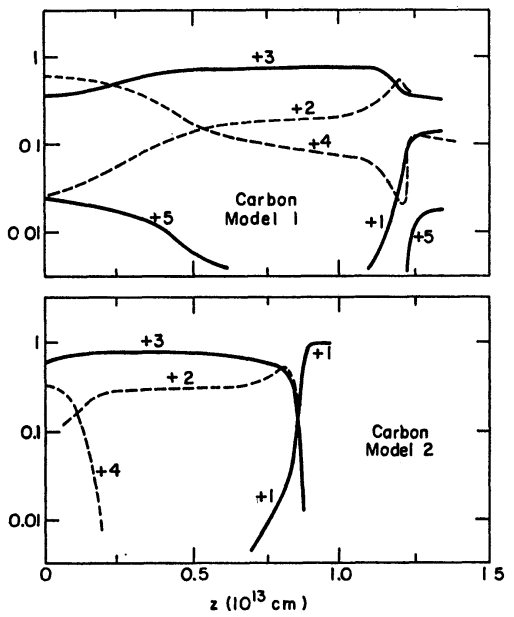

FIG 4

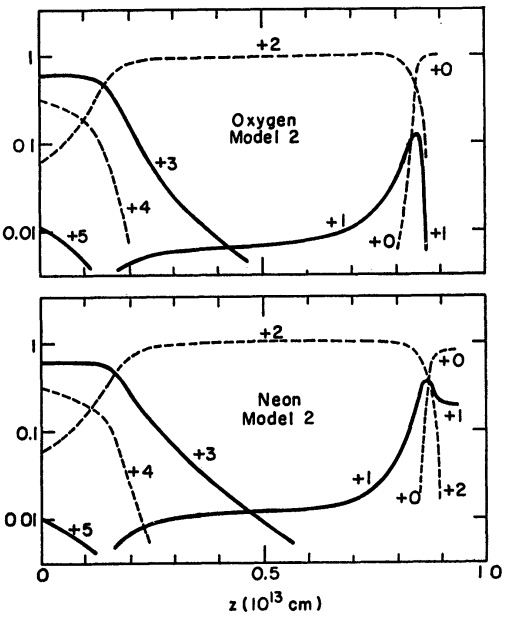

FIG 5

FIG. 4.—Ionization of carbon in Models 1 and 2.
FIG. 5.—Ionization of oxygen and neon in Model 2.

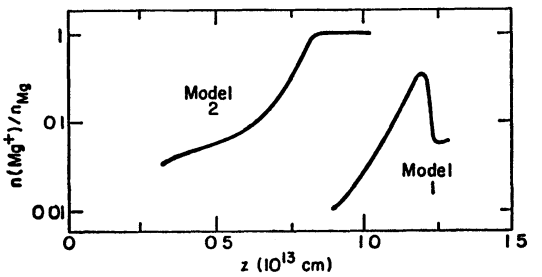

FIG. 6.—Fraction of magnesium which is singly ionized in Models 1 and 2

TABLE 3

RELATIVE INTENSITIES IN MODELS 1 AND 2 (High-density gas)

Line	Model 1	Model 2	Line	Model 1	Model 2
C III λ977..	0.7	0.4	N III] λ1747 .	≥0.15:	≥0.17:
O VI λ1034.....	0.6	0.1	C III] λ1909 .	2 6	2.8
H I λ1215 .	56.	50	Mg II λ2798	1.0:	2.9
N V λ1240	1.4	< 0.1	[Ne V] λ3426..	0.24	0.02
O IV] λ1406	≥ 0.6:	≥ 0.14:	[Ne III] λ3868	0.15	0 24
N IV] λ1488..	1.1	0.6	[O III] λ4363	0 20	0 22
C IV λ1549.. .	23.	12.	He II λ4686 .	0.16	0.06
He II λ1640	1.3	0.5	H I λ4861 . .	1 00	1 00
O III] λ1663	≥ 0.4:	≥ 0.5:	[O III] λ5007	0.14	0 18

absolute reference, the ratio (emitted Hβ)/(total incident ionizing flux) is 0.0058 for Model 1 and 0.011 for Model 2. The most important lines, as expected, are Lα, C IV λ1549, C III] λ1909, and Mg II λ2798. These are to be compared with the desired intensities listed in Table 2.

Consider Model 1 first. About 38 percent of the Lα is due to collisional excitation. $I(\mathrm{L}\alpha)/I(\mathrm{H}\beta)$ is larger than in Table 2—but this is not very significant because it is not a directly observed quantity. Of more interest are the ultraviolet-line ratios I(C IV λ1549)/I(Lα) and I(C IV λ1549)/I(C III] λ1909), which are both too large in Model 1. As stated in § IV above, these ratios depend upon $U_1 = F_1/n_e$ and would become approximately correct if U_1 were reduced by a factor of about 2.

Model 2 has nearly the same value of U_1 as Model 1; but since it has fewer high-frequency photons, it produces a somewhat different line spectrum. About 30 percent of the Lα intensity is due to collisional excitation, and the relative intensities of Lα, C IV λ1549, C III] λ1909, and Mg II λ2798 are not much different from those in Table 2. These lines are all more intense, relative to Hβ, than in Table 2; but of course the ultraviolet/visual calibration may be wrong in Table 2. Note also that as expected, the He II recombination lines are fainter in Model 2 than in Model 1.

In order to provide the observed [O III] λ5007 intensity, Models 1 and 2 must be supplemented by a lower-density component. Model 3 is intended to accompany Model 2 for this purpose. Here the assumed configuration is spherically symmetric, with gas of uniform density $n_{\mathrm{H}} = 3 \times 10^4\ \mathrm{cm}^{-3}$ outside a boundary of radius $R_0 = 10^{19}$ cm = 3.2 pc. Abundances are the same as in Model 2. A central radiation source produces an ionizing spectrum of the same shape as in Model 2, with total ionizing luminosity 10^{45} ergs s^{-1}, so that $F_1 = 2.8 \times 10^{16}$ Ryd Ryd^{-1} cm^{-2} s^{-1} at the inner boundary of the gas. This luminosity is quite small by QSO standards; but an increased luminosity with a correspondingly larger ionized region would lead to almost identical relative line intensities. Stratification is quite distinct in Model 3 because U_1 is large, and collisional de-excitation is negligible because n_e is small; under such conditions, the line spectrum is insensitive to the precise values of U_1 and n_e and also to the geometrical situation. Only the abundances and the form of the ionizing spectrum are crucial.

Figure 7 shows the electron temperature and the ionization of hydrogen and helium in Model 3, as functions of distance R from the central source. He III extends to $R = 1.8 \times 10^{19}$ cm, and the limit of the H II is $R = 2.9 \times 10^{19}$ cm. Because of a lack of efficient cooling agents, the temperature in the He III zone is high. Most of the He II zone is cooler than in Model 2, since [O III] cooling is effective below $n_e \sim 10^6\ \mathrm{cm}^{-3}$; but the temperature rises near the ionization front, where most of the photons just below $\nu = 4$ Ryd are absorbed and where (unlike Model 2) there is little neutral hydrogen to provide additional cooling. The amount of neutral helium in Model 3 has been reduced by the assumption that if recombination produces a helium atom in a triplet state, photons below the Lyman limit will immediately cause reionization (Hummer 1968). This occurs only because U_1 is large, and has little effect upon the calculated line intensities.

Figure 8 shows the ionization structure of oxygen and neon in Model 3. Dielectronic recombination has been included and is important in the most highly excited zones. In particular: if O VI → O V dielectronic recombinaiton were neglected, the amount of O V would be reduced; and the consequent lower opacity just above $\nu = 9$ Ryd would lead fo the ionization of most of the Ne V—severely reducing the [Ne V] λ3426 line.

Burbidge *et al.* (1966) have noted a possible effect which could drastically modify the O III in Model 3. Ionizing photons with energies up to $\nu = 4$ Ryd are found in the O III zone; and these might ionize O III ions which have been excited to the metastable forbidden-line levels. Therefore, if the ionizing flux is sufficient, much of the O III could be replaced by O IV. The flux in Model 3 is indeed large enough for this effect to be significant; however, it is assumed that the He II Lδ, Lε, etc., absorption lines blanket the relevant frequencies just below 4 Ryd, provided that each doppler width corresponds to

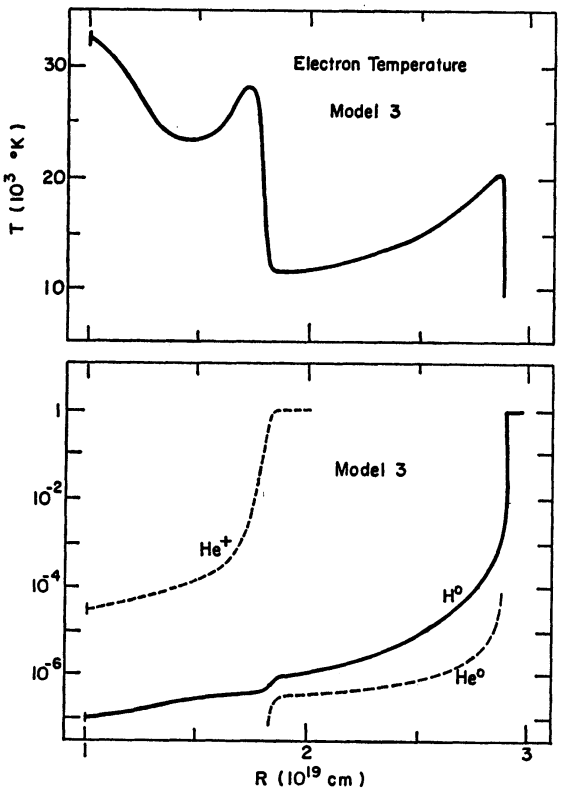

FIG 7

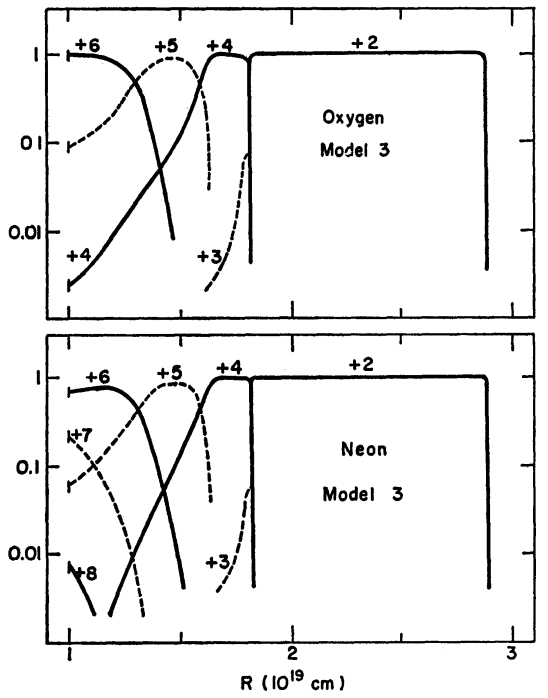

FIG 8

FIG. 7.—Temperature and ionization of hydrogen and helium in the spherically symmetric ionized region of Model 3, representing a low-density component (see § V).

FIG. 8.—Oxygen and neon ionization in Model 3.

1000 km s^{-1} or more. A related process, also neglected here, has been mentioned by Burgess (1967).

The major lines produced in Model 3 are listed in Table 4. Column (2) gives the relative intensities produced by the complete, ionization-limited H II region, while column (3) gives values which result if the outer layers beyond $R = 2.35 \times 10^{19}$ cm are removed; this truncated version is motivated chiefly by the observed [Ne V] λ3426 intensity, which

TABLE 4

RELATIVE INTENSITIES IN MODEL 3 (Low-density gas)

Line	Complete Region*	Inner Portion†	Line	Complete Region*	Inner Portion†
O VI λ1034.	2 4	4.6	[Ne V] λ3426	0 7	1.4
O V] λ1214.	1 2	2.3	[Ne III] λ3868	2 4	1 1
H I λ1215.	35.	35.	[O III] λ4363	0 5	0.13
N V λ1240	0.4	0.8	He II λ4686	0.07	0.13
C IV λ1549.	15	3.6	H I λ4861	1.00	1.00
He II λ1640	0.7	1.3	[O III] λ5007	25 3	12.5

* Outer boundary 2.9×10^{19} cm; Hβ luminosity 0.8×10^{43} ergs s^{-1}.

† Outer boundary 2.35×10^{19} cm; Hβ luminosity 0.4×10^{43} ergs s^{-1}

must be comparable to that of [Ne III] λ3868. Since the denser component (Model 2) contains little Ne V, evidently the [Ne V] line must originate in the less-dense gas (Model 3); but column (2) of Table 4 shows that the complete low-density ionized region gives a small $I(\lambda 3426)/I(\lambda 3868)$ ratio. Furthermore, other calculations have shown that any change in the slope of the ionizing spectrum would be likely to *decrease* the relative size of the Ne V zone. Hence, the desired line ratio can be obtained only by reducing the [Ne III] line intensity, by limiting the extent of the Ne III zone. Column (3) of Table 4 demonstrates this possibility; the exact outer boundary is, of course, somewhat arbitrary.

The complete two-component model is some mixture of Models 2 and 3; for example, Model 2 might represent small dense clouds distributed throughout the relatively tenuous gas of Model 3. The resultant line spectrum (ignoring the small effects due to shadowing of one component by the other) is a linear combination of Model 2 in Table 3 and column (3) of Table 4, with relative proportions adjusted to give the desired $I([\text{O III}]\ \lambda 5007)/I(\text{H}\beta)$ ratio. Table 5 lists such a spectrum, in which 85 percent of the Hβ intensity is due to Model 2 and 15 percent is due to the truncated Model 3. (These relative proportions imply simply that the dense component absorbs more ionizing photons than the less dense gas.) This spectrum agrees fairly well with the typical observed intensities—especially if the adopted ultraviolet/visual calibration in Table 2 is slightly wrong. Modest revision of some parameters would improve the model further: for example, [O III] λ4363 originates mostly in the hotter, denser component, where collisional de-excitation is significant; and so this line could be reduced by increasing the density (and also the radiation flux, to keep U_1 constant). Such an increase in density would also reduce [Ne III] λ3868, making it more nearly equal to the [Ne V] λ3426 line emitted by the more tenuous component; then an increased neon abundance would bring both lines into close agreement with Table 2.

The one notable failure of the two-component model involves [O II] λ3727, which is observed in some QSO spectra but whose predicted intensity is negligible. This line cannot originate in high-density gas, since collisional de-excitation sets in above $n_e \sim 10^4$ cm^{-3}; but also, with the adopted ionizing-spectrum shape, O II occurs only where $U_1 = F_1/n_e$ is small. Together, these considerations indicate that the [O II] doublet must come from gas which is at least several hundred parsecs from the source of ionizing radiation. Perhaps this suggests that the less dense component is actually more tenuous and more

TABLE 5

RELATIVE LINE INTENSITIES IN TWO-COMPONENT MODEL
(85% Model 2 + 15% truncated Model 3)

Line	Calculated Intensity	Desired Intensity (Table 2)	Line	Calculated Intensity	Desired Intensity (Table 2)
C III λ977	0.3	.	N III λ1747	≥0 1:	.
O VI λ1034	0.7*	...	C III] λ1909	2.4	2
O V] λ1214	0.3*		Mg II λ2798	2.5	1.5
H I λ1215	48	40	[Ne V] λ3426	0.23*	0.4:
N V λ1240	0.2*	. .	[O II] λ3727	<0.01	0.2:
O IV] λ1406	≥ 0.1:		[Ne III] λ3868	0.37	0.4:
N IV] λ1488	0.5	.	[O III] λ4363	0.2	≲0.2
C IV λ1549	11.	9	He II λ4686	0.07	≲0.3
He II λ1640	0.6	≤ 3	H I λ4861	1 00	1.00
O III] λ1663	≥ 0.4:	..	[O III] λ5007	2.0*	2.0

* Denotes lines which originate primarily in the less dense component.

distant from the central source than in Model 3 above; or perhaps there may be a third component or a more widespread continuous distribution of gas—the observed lines do not discriminate among these possibilities.

While the above two-component model illustrates one possible QSO-like situation, it is not necessarily unique in producing satisfactory emission lines. Leaving the question of abundances to be discussed in § VI, one may consider possible modifications in the ionizing spectrum and gas densities. The assumed ionizing spectrum which excites the two-component model above is characterized by a progressive high-frequency cutoff, due to an exponential factor. Such a cutoff reduces the He II recombination line intensities and can be used to adjust these lines into agreement with particular observed QSO spectra. Model 1 has demonstrated the larger He II intensities resulting from an ordinary power-law spectrum, which may be satisfactory for certain objects—although the Mg II λ2798 line would then seem harder to explain. The high-frequency spectrum also affects the amount of Ne V present.

The gas density in the less dense component was chosen almost arbitrarily; if $n_e \lesssim 3 \times 10^5$ cm^{-3}, the electron temperature and the emitted line spectrum are insensitive to n_e. In the dense component, however, collisional de-excitation of forbidden lines is important and the forbidden-line intensities listed in Table 3 are roughly proportional to n_e^{-1}. Consequently, a reduction in density would cause [O III] λ4363 and [Ne III] λ3868 to become undesirably bright (see Tables 3 and 5). This suggests that with the adopted abundances, densities of the order of 10^8 cm^{-3} or more should be present.

Finally, the value of $U_1 = F_1/n_e$ is approximately determined for the dense component, since it affects the relative intensities of Lα, C IV λ1549, and C III] λ1909. The value in the above model is of the order of $U_1 \sim 3 \times 10^8$ cm s^{-1}. In the more tenuous component, U_1 is larger and indeterminate.

VI. POSSIBLE LOW ABUNDANCES

As implied in § IV above, major alterations of elemental abundances are worth contemplating for at least two different reasons: a scarcity of heavy ions may raise the electron temperature, causing the observed forbidden/permitted line ratios to occur even at low densities; and the weakness of He II λ4686 in some QSO spectra may be due to a lack of helium rather than of high-frequency photons. Two calculations will be described here in order to illustrate these possibilities and their difficulties; but unlike § V, no attempt will be made to match the observed lines in detail.

Model 4 assumes a normal helium abundance ($n_{He} = 0.07 n_H$) but reduced heavy-element abundances: $n_Z/n_H = (0.7, 0.4, 1.3, 0.4) \times 10^{-5}$ for Z = (C, N, O, Ne). The gas is distributed outside a boundary $R_0 = 2 \times 10^{19}$ cm, not homogeneously but rather as many small filaments or clouds, each optically thin, and collectively occupying 4 percent of the volume outside R_0. (This simplified nonuniformity, which is similar in principle to the filling factor used by Bahcall and Kozlovsky 1969*a*, was adopted partly for calculative convenience; a uniform, thin-shell model near $R \approx 6 \times 10^{19}$ cm would lead to a similar spectrum.) Within each cloud or filament the hydrogen density is the same as in Model 3, $n_H = 3 \times 10^4$ cm^{-3}. (This, rather than the volume-averaged density of about 1200 cm^{-3}, is the appropriate value to use in considering the parameter $U_1 = F_1/n_e$.) The central ionizing source in Model 4 is identical to that of Model 3: $F_\nu \sim \nu^{-0.5} e^{-0.5\nu}$, with 10^{45} ergs s^{-1} beyond $\nu = 1$ Ryd.

The calculated ionization structure of Model 4 is shown in Figures 9 and 10. The temperature is higher than in Model 3, since the cooling efficiency is lower. Also unlike Model 3, the heavy ions in the He III zone are not stratified into distinct zones; this is partly because photons beyond $\nu \approx 8$ Ryd are absorbed by helium rather than by O V and O VI as in Model 3.

Relative line intensities produced in Model 4 are listed in Table 6. Column (2) gives

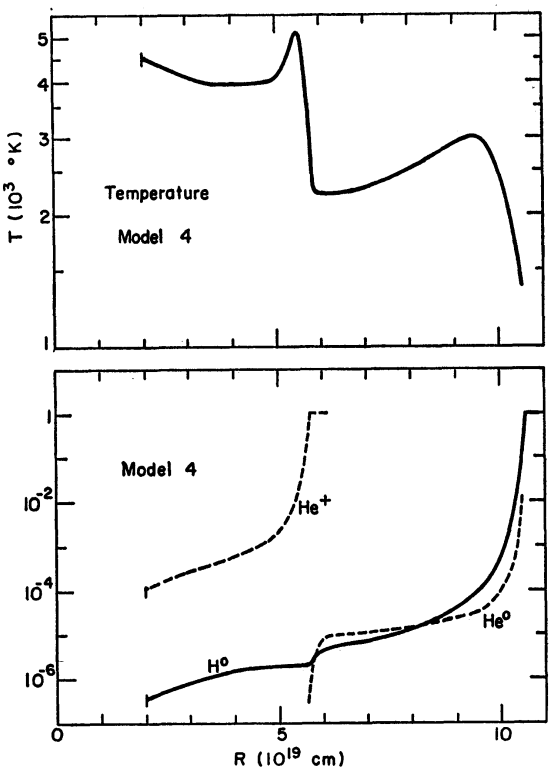

FIG 9

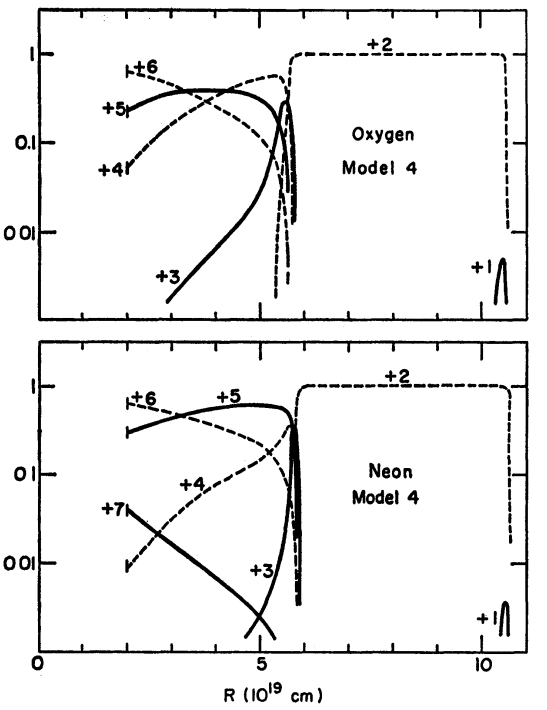

FIG. 10

FIG. 9.—Temperature and ionization of hydrogen and helium in Model 4, which has low densities and small C, N, O, Ne abundances (see § VI).

FIG. 10.—Oxygen and neon ionization in Model 4.

TABLE 6

RELATIVE INTENSITIES IN MODEL 4 (Low C, N, O, Ne abundances)

Line	Complete Region*	Inner Portion†	Line	Complete Region*	Inner Portion†
O VI λ1034	0.9	2.3	O III] λ1909	0.34	0.11
O V] λ1214	0.27	0.7	[Ne V] λ3426	0.03	0.07
H I λ1215	42	36	[Ne III] λ3868	0.6	0.4
N V λ1240	0.25	0.6	[O III] λ4363	0.15	0.11
N IV] λ1488	0.7	0.5	He II λ4686	0.04	0.09
C IV λ1549	9	7	H I λ4861	1 00	1.00
He II λ1640	0.5	1.3	[O III] λ5007	3.9	3.0
O III] 1663	≥0.25:	≥0 17:			

* Outer boundary ≥10 6 × 10^{19} cm; Hβ luminosity 1 0 × 10^{43} ergs s^{-1}

† Outer boundary 8.0 × 10^{19} cm; Hβ luminosity 0.4 × 10^{43} ergs s^{-1}.

the results for the entire, ionization-limited H II region, while in column (3) the gas outside $R = 8 \times 10^{19}$ cm has been removed. The Lα, C IV, [O III], and [Ne III] lines are roughly consistent with Table 2 and would be better if there were less oxygen. However, C III] λ1909 is seriously deficient; and Mg II λ2798, which has not been calculated, would probably be similar. To account for these lines, some gas must have smaller values of U_1, entailing larger n_e or greater distance from the ionizing source; but regions with small U_1

would also tend to produce additional collisionally excited Lα. Another difficulty is the calculated weakness of [Ne v] λ3426. Despite these obstacles, it seems fair to say that a nonuniform, low-density model, with low heavy-element abundances resembling extreme Population II, might conceivably produce a QSO-like spectrum.

A fairly conventional helium abundance has been assumed in each calculation described above; the exact value has very little effect upon any observed line except perhaps [Ne v] λ3426. However, as outlined in § IV above, if n_{He}/n_H is smaller than about 0.01 (depending somewhat upon the ionizing spectrum), the situation becomes qualitatively different because the He III zone then occupies the entire H II region. In this case the helium recombination-line intensities depend upon the helium abundance while the intensities of C IV, [O III], and [Ne III] lines may suffer from the disappearance of the He II zone which normally produces them. Bahcall and Kozlovsky (1969*a*, *b*) have described some models of this type, in which helium is quite scarce and C III, C IV, O III, and Ne III are present only because U_1 is small.

Model 5 is a plane-parallel configuration with $n_{He}/n_H = 0.007$, down by a factor of 10 from the other models. The heavier elements are moderately abundant: $n_Z/n_H = (1.5, 1.0, 3.0, 1.0) \times 10^{-4}$ for Z = (C, N, O, Ne). The uniform density is $n_H = 10^6$ cm^{-3}, and the incident spectrum is $F_\nu \sim \nu^{-1\,4}$, $F_1 = 2.5 \times 10^{14}$ Ryd Ryd^{-1} cm^{-2} s^{-1}; this is equivalent to the flux at a distance of 7.8 pc from a source whose ionizing luminosity is 10^{46} ergs s^{-1}. The calculation is comparable to some of the models of 3C 48 by Bahcall and Kozlovsky, except that U_1 is smaller—this change being necessary because most of the adopted photoionization cross-sections are much larger at high frequencies than those used by Bahcall and Kozlovsky, who did not include ionization involving inner electron shells. The resultant temperature and ionization structure are shown in Figures 11 and 12. Throughout the configuration, several stages of ionization coexist for each element. The calculation extends to $z = 2 \times 10^{15}$ cm, where the gas is still optically thin for $\nu > 20$ Ryd; clearly the X-ray photons can penetrate far beyond this point.

Table 7 lists the line intensities produced in Model 5, under the assumption of two different outer boundaries. The Lα, C IV, C III], and [O III] lines are not implausible; and, as intended, He II λ4686 is faint. However, [Ne v] λ3426 is too intense and [Ne III] λ3868 is too weak; while Mg II (not calculated) would probably be as scarce as Ne I or Ne II, which have similar high-frequency photoionization cross-sections. An extensive partially-ionized H I region would convert some of the remaining X-ray flux into Lα, Mg II λ2798, and [O I] λ6360. Model 5, like Model 4, should be regarded as a partial representation of a marginally possible QSO-like situation.

Finally, it might be natural to consider a model in which both helium and the heavier elements are simultaneously underabundant. But if the heavy elements were reduced in Model 5, the carbon and oxygen lines would certainly become too faint, relative to Lα and Hβ; apparently such a model would be unsatisfactory. (This is confirmed by other calculations not described here.)

VII. DISCUSSION

The calculations described above are unfortunately indecisive, for they seem to indicate that elemental abundances cannot be uniquely estimated from the few known lines in a QSO spectrum. C, N, O, Ne, and Mg may have abundances as high as in galactic Population I objects (but not higher) or as low as in extreme Population II (but not much lower). Some QSOs have appreciable amounts of helium, since the He II recombination lines are present; but a few objects (notably 3C 273) must have a scarcity either of helium or of photons beyond $\nu = 4$ Ryd.

The spectrum of 3C 273 is remarkable for the extreme faintness (or absence) of the He II λ4686 line. Thus Bahcall and Kozlovsky (1969*a*) concluded that $n_{He}/n_H < 0.01$; or, in an alternative model of the type described in § V above, the ionizing spectrum must become very steep near 4 Ryd. Bowyer *et al.* (1970) have observed an X-ray flux from 3C 273 which, if connected to the visual flux by a rather moderate power law,

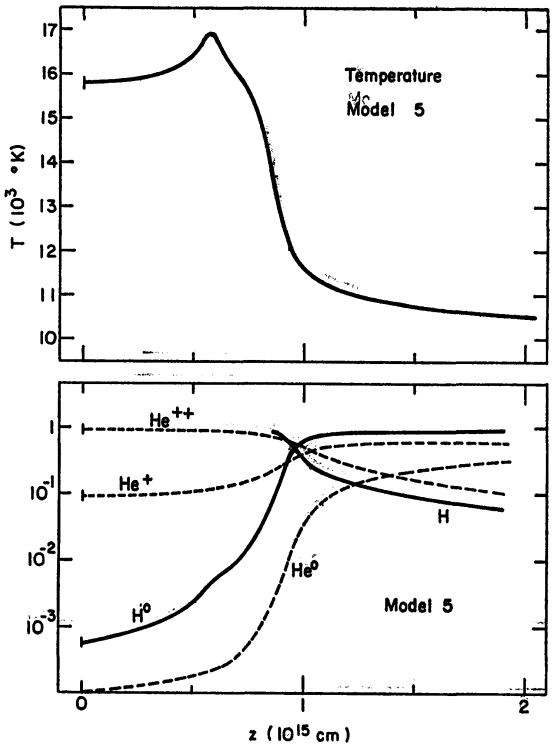

FIG. 11

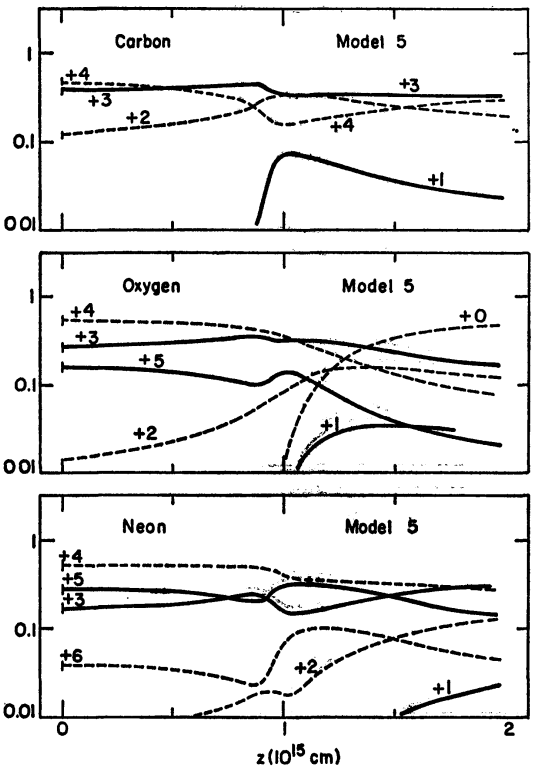

FIG. 12

FIG. 11.—Temperature and ionization of hydrogen and helium in Model 5, where the helium abundance is small (see § VI).

FIG. 12.—Carbon, oxygen, and neon in Model 5.

TABLE 7

RELATIVE INTENSITIES IN MODEL 5 (Low helium abundance)

Line	A*	B†	Line	A*	B†
C III λ977.	0.3	0.3	C III] λ1909.....	2.0	2.1
O VI 1034.	0.3	0.3	[Ne IV] λ2424...	0.19	0.21
O V] λ1214. .	0.4	0.5	[Ne V] λ3426...	2.4	2.5
H I λ1215	56	69	[Ne III] λ3868. . .	0.05	0.08
N V λ1240.	1.2	1.2	[O III] λ4363.. ..	0.03	0.03
O IV] λ1406	0.3:	0.3:	He II λ4686.....	0.05	0.06
N IV] λ1488..	0.6	0.6	H I λ4861.....	1.00	1.00
C IV λ1549.....	8.8	9.0	[O III] λ5007	0.55	0.9
He II λ1640....	0.39	0.42	[O I] λ6360.. ...	<0.05	0.1:

* Outer boundary $z = 1.0 \times 10^{15}$ cm; fraction of ionizing flux converted to Hβ, 0.0063.
† Outer boundary $z = 2.0 \times 10^{15}$ cm; fraction of ionizing flux converted to Hβ, 0.0066.

seems inconsistent with the steep ionizing spectrum proposed above. However, a power-law interpolation is not inevitable, especially since the visual continuum is much flatter than such a power law—the spectrum may instead have something like an exponential cutoff between $\nu = 1$ Ryd and $\nu = 4$ Ryd, followed by a lower, flatter contribution at higher frequencies to include the X-ray flux. (Then the infrared, ultraviolet, and X-ray

continua might resemble three descending steps, inducing thoughts about inverse Compton radiation.) It is necessary also to remember that such processes as collisional excitation of hydrogen may preclude any simple photoionization analysis. Possibly, the He I recombination lines, which originate in a zone containing He II and which are faint in all models, might eventually be detectable if the helium abundance is not low.

For a QSO with a conventional helium abundance, the most plausible type of model is that described in § V above. If the heavy elements have the assumed abundances, then some electron densities must be of the order of 10^8 cm^{-3}. Since the parameter U_1 has been estimated, it is possible to deduce the maximum thickness of a photoionized region having such a density; and the result, as in Models 1 and 2, is of the order of 10^{13} cm, or about 1 a.u. This surprisingly small size scale evidently requires some explanation, as the characteristic time for free expansion would be less than a year.

One possible situation leading to such conditions involves a system of dense sheets, formed by shock fronts. Consider, for example, a head-on collision of two similar clouds, each having an internal density of about 10^5 cm^{-3} and moving at a relative speed of 1000 km s^{-1}. The layers near the collision interface are compressed, and a shock front moves through each cloud as the collision continues. As material passes through one of these fronts, it is adiabatically heated to about 3×10^6 ° K, but then cools radiatively in less than 10 years, while being compressed further, until it falls to the equilibrium temperature maintained by photoionization. The density in the sheet of cooled, photoionized gas between the shock fronts is approximately

$$n_e \approx (10^5 \text{ cm}^{-3}) \left(\frac{500 \text{ km s}^{-1}}{w}\right)^2 ,$$

where w, the sound speed in the photoionized gas, is of the order of 15 km s^{-1}. Therefore, $n_e \approx 10^8$ cm^{-3}, as required. It is possible to envision a large number of fast-moving clouds in a region several parsecs across, forming dense sheets by collisions in this manner. One may naturally identify the compressed sheets with the denser component of § V (i.e., Model 2) and the undisturbed clouds with the tenuous component (Model 3). Osterbrock and Parker (1965) and Nussbaumer and Osterbrock (1970) have discussed similar situations in connection with Seyfert galaxies, emphasizing the role of the collisionally heated gas near each shock front. The hot gas would emit soft X-rays; but with likely parameters the resulting X-ray flux entering each cooled, dense photoionized layer is less than the previously assumed incident flux, which must be produced elsewhere in the QSO. The colliding-cloud model may crudely represent a more complicated pattern of shock fronts and supersonic turbulence; also, strong magnetic fields embedded in the gas would inhibit the necessary compression.

An alternative scheme would suppose that many small clouds of gas are in pressure equilibrium with a flux of energetic particles or radiation produced in the QSO, leading to densities of 10^8 cm^{-3}. Several authors have proposed that much of the energy output comes from pulsar-like objects—either single large spinning objects (Morrison 1969; Cavaliere, Pacini, and Setti 1969) or swarms of ordinary pulsars (Gunn and Ostriker 1970; Rees 1971). In such cases much of the energy flux is in the form of low-frequency electromagnetic fields. A cloud of gas, opaque at such frequencies, would be compressed by such radiation until the gas pressure is similar to the electromagnetic pressure. If one conjectures that the ionizing radiation intensity depends upon position in roughly the same manner as the pulsar radiation, then $U_1 = F_1/n_e$ automatically becomes rather uniform throughout a particular object. An interesting relation may be noted: if p_{gas} and $p_{i\,\text{rad}}$ are the pressures of the photoionized gas and the ionizing radiation, then

$$(p_{i\,\text{rad}}/p_{\text{gas}}) \approx (I_{\text{H}}/2kT)(U_1/c) \approx 5U_1/c ,$$

where $I_H = 1$ Ryd $= 13.6$ eV. If $U_1 \approx 3 \times 10^8$ cm s^{-1} as suggested in § V above, the gas pressure is roughly 20 times as large as the ionizing radiation and perhaps comparable to the total radiation pressure. Is this more than coincidence?

I am grateful to a number of people for many useful discussions: primarily E. E. Salpeter, and also W. H. Tucker, L. Spitzer, Jr., T. Gold, J. N. Bahcall, and C. B. Tarter. Some of this work was supported by an NSF Graduate Fellowship and NSF grant GP-26068 at Cornell University, and some was supported by NASA grant NGL-31-001-007 at Princeton University.

APPENDIX

TRANSFER OF SECONDARY IONIZING RADIATION

As explained in § II, for each iteration of the photoionization calculation it is necessary to find the distribution of secondary radiation in a spherical configuration. For present purposes, an unsophisticated approach was judged sufficient and appropriate. Consider some particular narrow frequency interval, and let $I(\mu)$ denote the intensity in this interval at direction-cos μ (outward, $+1$). Denote the coefficients for photoionization-absorption and electron scattering by κ_a and κ_s, while $\kappa = \kappa_a + \kappa_s$ is the total. Let ϵ represent the local secondary radiation production per unit volume within the frequency interval, plus a contribution due to scattering of the outward-moving primary beam. The equation of transfer is

$$\mu \frac{\partial I}{\partial r} + \frac{(1 - \mu^2)}{r} \frac{\partial I}{\partial \mu} = -\kappa I + \kappa_s J + \frac{\epsilon}{4\pi}, \tag{A1}$$

where r is the radial position and $J = \frac{1}{2}\int I d\mu$ (the integration is from -1 to $+1$). Let H and K represent the next two moments of I with respect to μ, in the usual fashion; then the flux equation results from integrating equation (A1) through μ:

$$\frac{1}{r^2} \frac{d}{dr} (r^2 H) = -\kappa_a J + \frac{\epsilon}{4\pi}. \tag{A2}$$

Multiplying equation (A1) by μ, then integrating, we obtain

$$\frac{dK}{ar} + \frac{(3K - J)}{r} = -\kappa H. \tag{A3}$$

Adopting the Eddington approximation, $K = \frac{1}{3}J$. Then simply

$$\frac{dJ}{dr} = -3\kappa H. \tag{A4}$$

Equations (A2) and (A4) are to be solved, with given $\kappa(r)$ and $\epsilon(r)$. At the outer boundary, the condition is $H = \mu_b J$, where $\mu_b \approx 1/\sqrt{3}$. At the inner edge of a closed shell, the boundary condition is $H = 0$. But in a thin-shell approximation of a plane-parallel problem, the inner boundary is "open"; i.e., inward-moving photons escape when they pass the boundary. In such an approximation $H \approx -\mu_b J$ at that boundary.

If some value for J_{inner} at the inner boundary is assumed, straightforward integration leads to some outer-boundary value of $(H - \mu_b J)_{\text{outer}}$, which is nearly a linear function of J_{inner}. So by using Newton's method, with two or three trial values of J_{inner}, the appropriate value of J_{inner} is quickly found. Rounding errors cause this method to fail for large optical depths; but with certain precautions, the procedure is workable for treating the continuous radiation in an ionized region where the parameter U_1 is not too large.

REFERENCES

Allen, J. W., and Dupree, A. K. 1969, *Ap. J.*, **155**, 27.
Bahcall, J. N., and Kozlovsky, B.-Z. 1969*a*, *Ap. J.*, **155**, 1077.
———. 1969*b*, *ibid.*, **158**, 529.
Bahcall, J. N., and Oke, J. B. 1971, *Ap. J.*, **163**, 235.
Bahcall, J. N., and Wolf, R. A. 1968, *Ap. J.*, **152**, 701.
Bearden, A. J. 1966, *J. Appl. Phys.*, **37**, 1681.
Bell, K. L., and Kingston, A. E. 1967, *Proc. Phys. Soc.* (*London*), **90**, 31.
Bely, O., and Van Regemorter, H. 1970, *Ann. Rev. Astr. and Ap.*, **8**, 329.
Bergeron, J., and Souffrin, S. 1971, *Astr. and Ap.* (in press).
Biermann, L., and Lübeck, K. 1949, *Zs. f. Ap.*, **26**, 43.
Bowyer, C. S., Lampton, M., Mack, J., and Mendonca, F. de. 1970, *Ap. J.* (*Letters*), **161**, L1.
Burbidge, G. R., and Burbidge, E. M. 1967, *Quasi-stellar Objects* (San Francisco: W. H. Freeman & Co.).
Burbidge, G. R., Burbidge, E. M., Hoyle, F., and Lynds, C. R. 1966, *Nature*, **210**, 774.
Burgess, A., and Summers, H. P. 1969, *Ap. J.*, **157**, 1007.
Burgess, D. D. 1967, *Nature*, 216, 1092.
Cavaliere, A., Pacini, F., and Setti, G. 1969, *Ap. Letters*, **4**, 103.
Cox, D., and Tucker, W. 1969, *Ap. J.*, **157**, 1157.
Davidson, K., and Tucker, W. 1970, *Ap. J.*, **161**, 437.
Dupree, A. K. 1968, *Ap. Letters*, **1**, 125.
Field, G. B., and Steigman, G. 1971, *Ap. J.*, **166**, 59.
Greenstein, J. L., and Schmidt, M. 1964, *Ap. J.*, **140**, 1.
Gunn, J. E., and Ostriker, J. P. 1970, *Ap. J.*, **160**, 979.
Henry, R. J. W., and Williams, R. E. 1968, *Pub. A.S.P.*, **80**, 669.
Hidalgo, M. B. 1968, *Ap. J.*, **153**, 981.
Hummer, D. G. 1968, *Planetary Nebulae*, ed. D. E. Osterbrock and C. R. O'Dell (Dordrecht: D. Reidel Publishing Co.), p. 166.
Mathez, G. 1969, *Astr. and Ap.*, **3**, 127.
Morrison, P. 1969, *Ap. J.*, **157**, L73.
Nussbaumer, H., and Osterbrock, D. E. 1970, *Ap. J.*, **161**, 811.
Oke, J. B. 1965, *Ap. J.*, **141**, 6.
———. 1970, *Ap. J.* (*Letters*), **161**, L17.
Oke, J. B., Neugebauer, G., and Becklin, E. E. 1970, *Ap. J.*, **159**, 341.
Osterbrock, D. E. 1970, *Ap. J.*, **160**, 25.
Osterbrock, D. E., and Parker, R. A. R. 1965, *Ap. J.*, **141**, 892.
———. 1966, *ibid.*, **143**, 268.
Rees, M. J. 1971, *Nature*, **229**, 312.
Seaton, M. J. 1958, *Rev. Mod. Phys.*, **30**, 979.
Shklovskii, I. S. 1965, *Soviet Astr.—AJ*, **8**, 638.
Tarter, C. B. 1967, thesis, Cornell University.
Tarter, C. B., and Salpeter, E. E. 1969, *Ap. J.*, **156**, 953.
Tarter, C. B., Tucker, W. H., and Salpeter, E. E. 1969, *Ap. J.*, **156**, 943.
Tucker, W. H. 1969, (private communication).
Wampler, E. J. 1968, *Ap. J.*, **153**, 19.
Wampler, E. J., and Oke, J. B. 1967, *Ap. J.*, **148**, 695.
Williams, R. E. 1967, *Ap. J.*, **147**, 556.
———. 1971, *Ap. J.* (*Letters*), **167**, L27.